Supporting Information

Anchoring of halogen-cleaved organic ligands on perovskite surfaces

Juntao Hu[a, f†], Peng Chen[b†], Deying Luo[c*], Linjie Dai[d], Nan Chen[a], Shunde Li[b], Shiyu Yang[f], Zewei Fu[f], Dengke Wang[a], Qihuang Gong[b, g, h], Samuel D. Stranks[d, e], Rui Zhu[b, g, h*], Zheng-Hong Lu[a, c*]

[a]Department of Physics, Center for Optoelectronics Engineering Research, Yunnan University, 650091 Kunming, China.

[b]State Key Laboratory for Artificial Microstructure and Mesoscopic Physics, School of Physics, Frontiers Science Center for Nano-optoelectronics & Collaborative Innovation Center of Quantum Matter, Peking University, 100871 Beijing, China.

[c]Department of Materials Science and Engineering, University of Toronto, Toronto, M5G 3E4 Ontario, Canada.

[d]Cavendish Laboratory, University of Cambridge, Cambridge CB3 0HE, UK

[e]Department of Chemical Engineering and Biotechnology, University of Cambridge, Cambridge CB3 0AS, UK

[f]Center of Development and Research, Yunnan Tin Group (Holding) Co. Ltd, 650106 Kunming, P. R. China

[g]Peking University Yangtze Delta Institute of Optoelectronics, Nantong, 226010 Jiangsu, China.

[h]Collaborative Innovation Center of Extreme Optics, Shanxi University, Taiyuan, 030006 Shanxi, China.

[†]These authors contributed equally to this work.
*e-mail: deying.luo@utoronto.ca (D.L.); iamzhurui@pku.edu.cn (R.Z.); zhenghong.lu@utoronto.ca (Z.-H.L.).

Supplementary Text

The film thickness estimation using XPS

A thin layer a, with a thickness of d is stacked on a substrate B. Based on the Beer-Lambert law, the integrated signal intensity between 0 and d can be expressed[1]:

$$I_A = I_A^{\infty}\left[1 - \exp(-d/\lambda_{A,A}\cos\theta)\right] \quad (1)$$

where the I_A^{∞} is the photoelectron intensity measured on an infinite thick film A, $\lambda_{A,\,A}$ is the photoelectron effective attenuation length in the overlayer, and θ is the photoelectron take-off angle during the XPS measurement.

Assuming that the B substrate is thick enough, the signal from B arriving at B-A interface is defined as I_B^{∞}. In this case, the signal will be attenuated by passing through the overlayer A. The signal emerging is therefore given by:

$$I_B = I_B^{\infty}\exp(-d/\lambda_{B,A}\cos\theta) \quad (2)$$

Here, the $\lambda_{B,A}$ is the photoelectron effective attenuation length in layer A for electrons emitted from substrate B. The $\lambda_{A,A}$ is approximately equal to $\lambda_{B,A}$ since the kinetic energy of the interested photoelectron (such as N 1s) arising from both the overlayer and the substrate is roughly the same. Using transition then, the thickness of the film can be described as:

$$d = \lambda_{A,\,A}\cos\theta\ln[1 + I_A \cdot I_B^{\infty}/I_B \cdot I_A^{\infty}] \quad (3)$$

In Equation 3, the I_A/I_B can be directly acquired by deconvoluting core level XPS spectra, where the $I_A^{\infty}/I_B^{\infty}$ is the intensity ratio of the respective infinite thickness film. The photoelectron effective attenuation length λ for the organic materials is given below [2]:

$$\lambda = 0.00387E^{0.842} \quad (4)$$

Here, the E is the kinetic energy of the photoelectron. So, with the equations mentioned above, we can estimate the thickness that relies on the relative intensity of the XPS peak intensity [3].

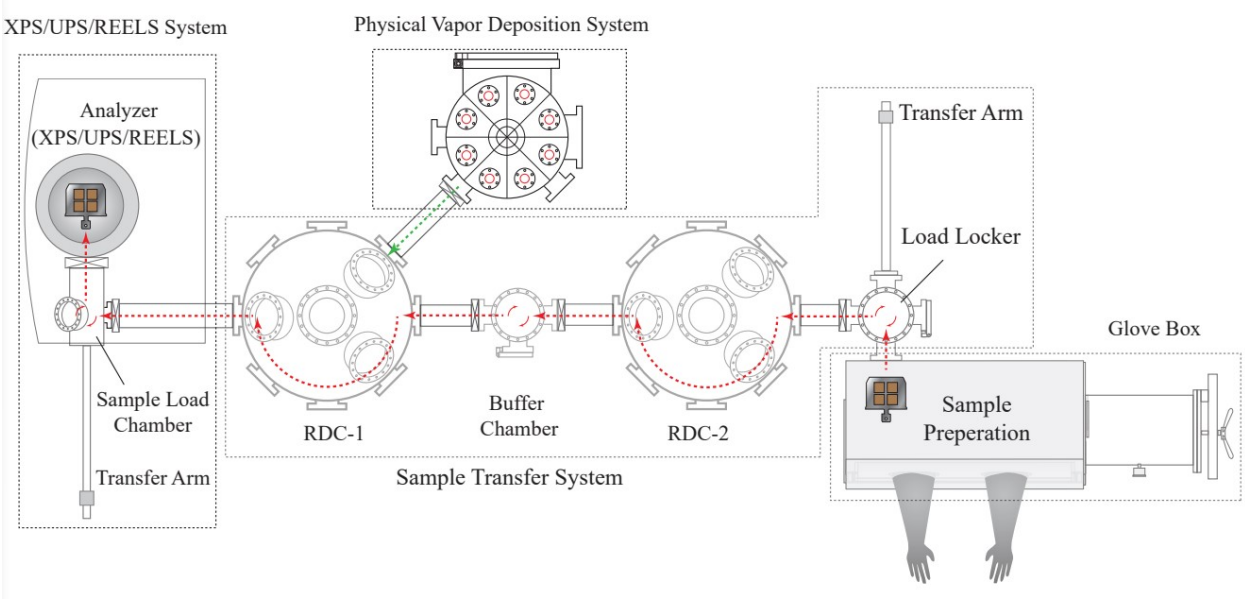

Fig. S1. The schematic diagram of a multi-linked system with the integrity of the sample preparation, sample transfer, and surface analyses. Note that all the sample preparation, layer-by-layer deposition, and measurements (in-situ XPS/UPS/REELS) were done in this multi-linked system. Red and green arrows represent the sample preparation and transfer from a glove box and a vapor-phase deposition chamber.

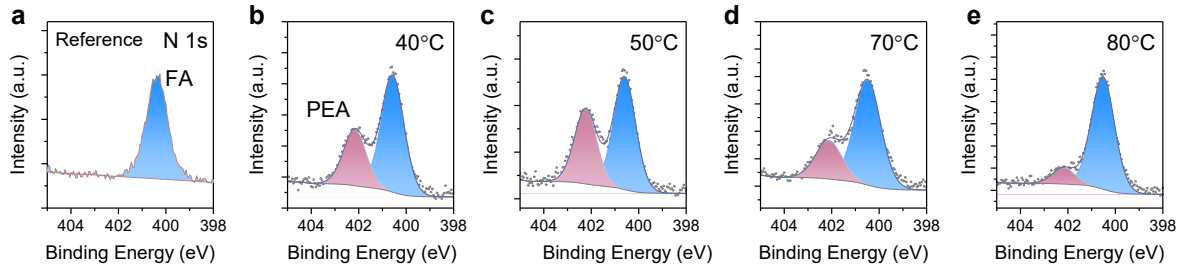

Fig. S2. (**a-e**) Curve fitting of core level N 1s XPS spectra of the perovskite without (reference) and with chlorinated-PEA-organics annealed at different temperatures.

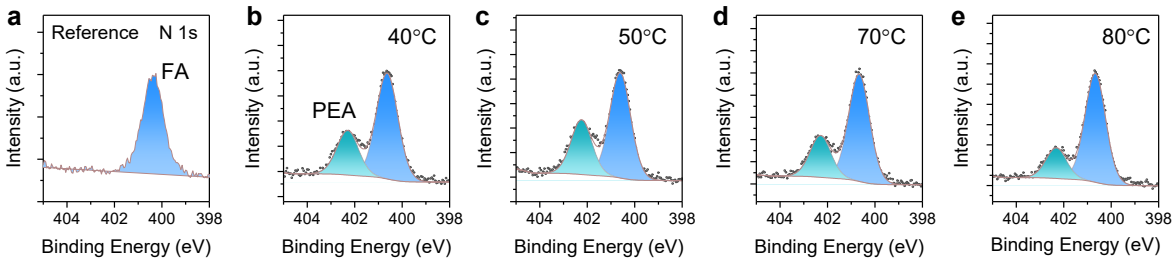

Fig. S3. (**a-e**) Curve fitting of core level N 1s XPS spectra of the perovskite without (reference) and with brominated-PEA-organics annealed at different temperatures.

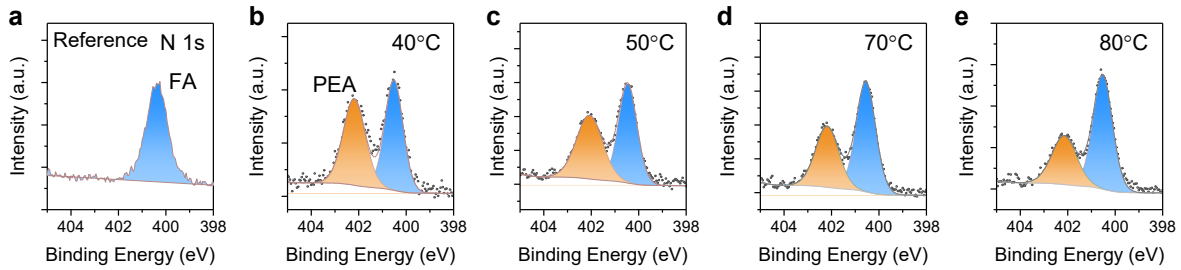

Fig. S4. (**a-e**) Curve fitting of core level N 1s XPS spectra of the perovskite without (reference) and with iodinated-PEA-organics annealed at different temperatures.

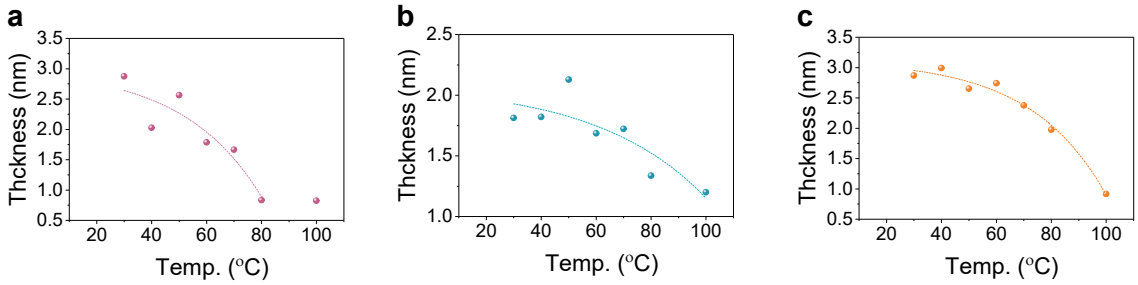

Fig. S5. Plots of the halogenated organic thickness versus temperature. **a**, Chlorinated PEA organic layers, **b**, Brominated PEA organic layer, and **c**, Iodinated PEA organic layer.

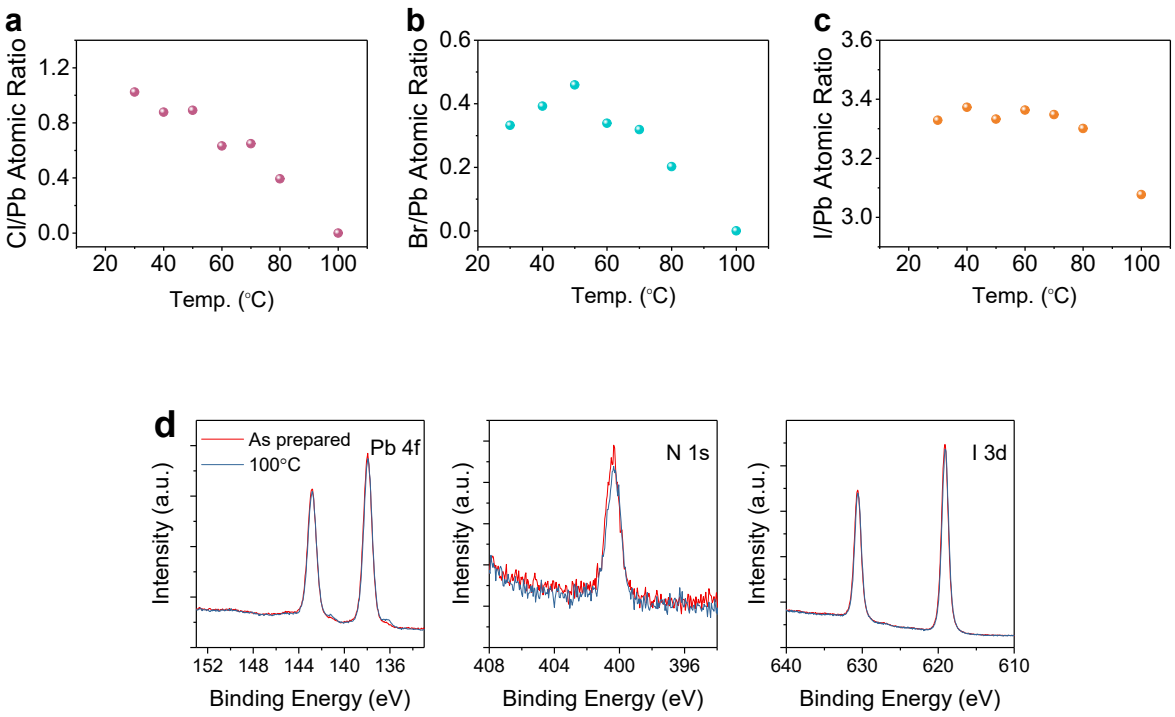

		Peak position eV	FWHM eV	Atomic %
As prepared	Pb4f	137.96	0.87	17.58
	N1s	400.4	0.93	28.03
	I3d	619.12	1.05	54.39
100°C	Pb4f	137.93	0.87	17.71
	N1s	400.31	0.99	28.16
	I3d	619.06	1.05	54.13

Fig. S6. Plots of the halide-to-lead atomic ratio versus temperatures. **a**, Cl/Pb atomic ratio. **b**, Br/Pb atomic ratio. **c**, I/Pb atomic ratio of the perovskite with the halogenated PEA organics. The halide-to-lead ratio shows gradual decrease trends with an increase in the post-annealing temperature. Cl/Pb atomic ratios of the perovskite with chlorinated-PEA-organic are estimated to be zero at 100°C. **d**, Pb 4f, N 1s and I 3d spectra of the control film before and after 100 °C annealing. Both contents and peak positions of the Pb, N and I were not varied.

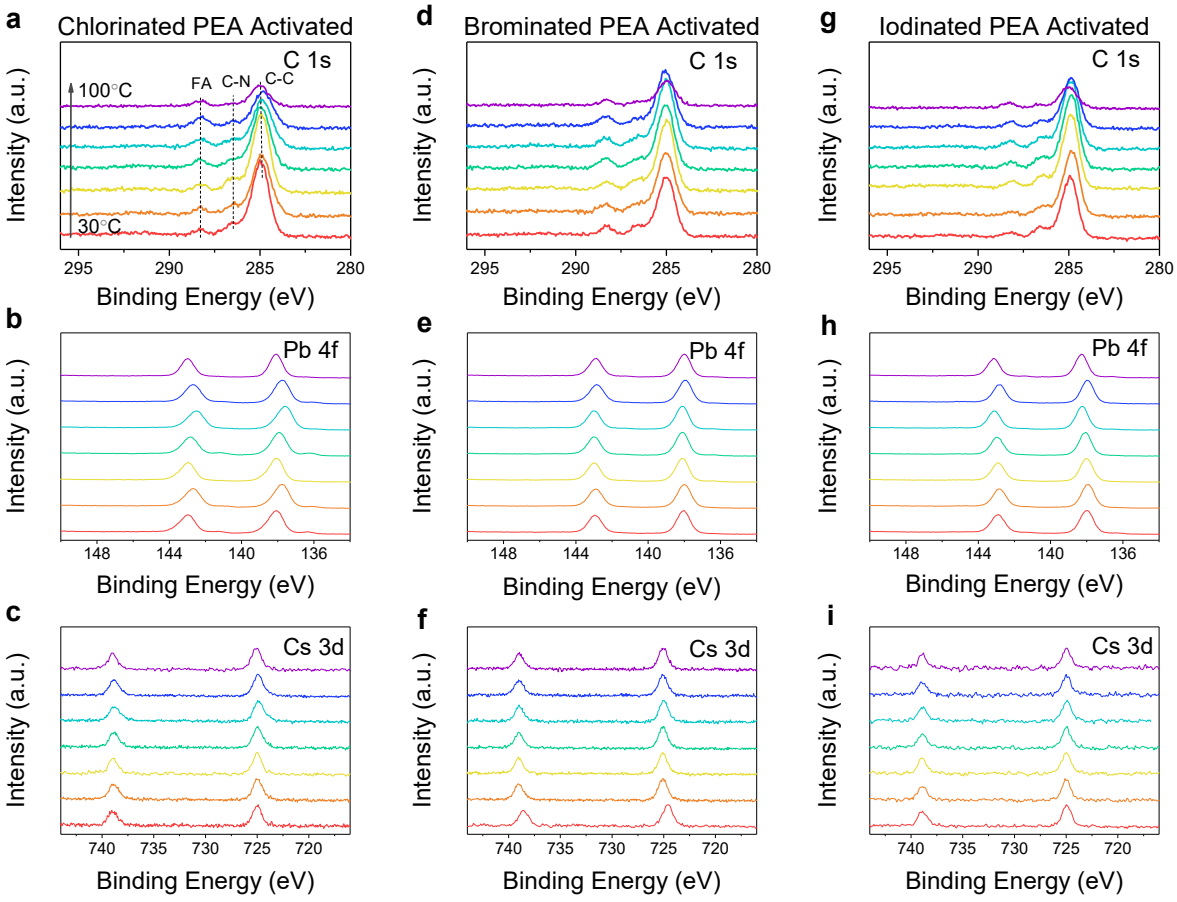

Fig. S7. Evolutions of XPS spectra of the perovskite with halogenated PEA organics over the temperatures. **a**, C 1s, **b**, Pb 4f, and **c**, Cs 3d of the perovskite with the chlorinated PEA organic layer. **d**, C 1s, **e**, Pb 4f, and **f**, Cs 3d of the perovskite with the brominated PEA organic layer. **g**, C 1s, **h**, Pb 4f, and **i**, Cs 3d of the perovskite with the iodinated PEA organic layer. The key peaks of the C 1s XPS spectra are indicated with chemicals in **a**.

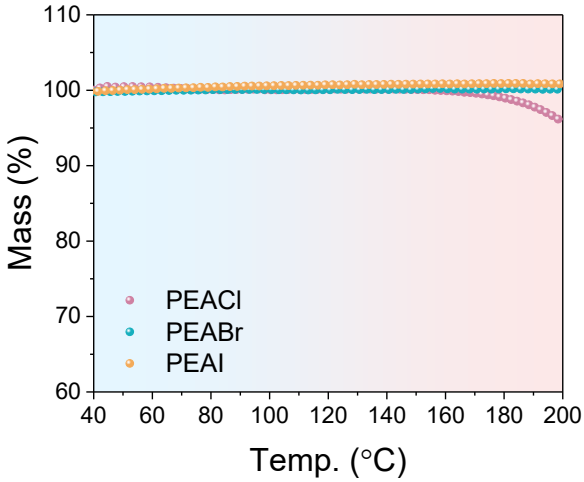

Fig. S8. TGA analysis for three types of halogenated PEA organic powders in an Ar atmosphere. The TGA analyses display that both PEABr and PEAI samples show a negligible mass loss over the temperature, while there has been a slight loss for the PEACl sample when the temperature is over 160℃.

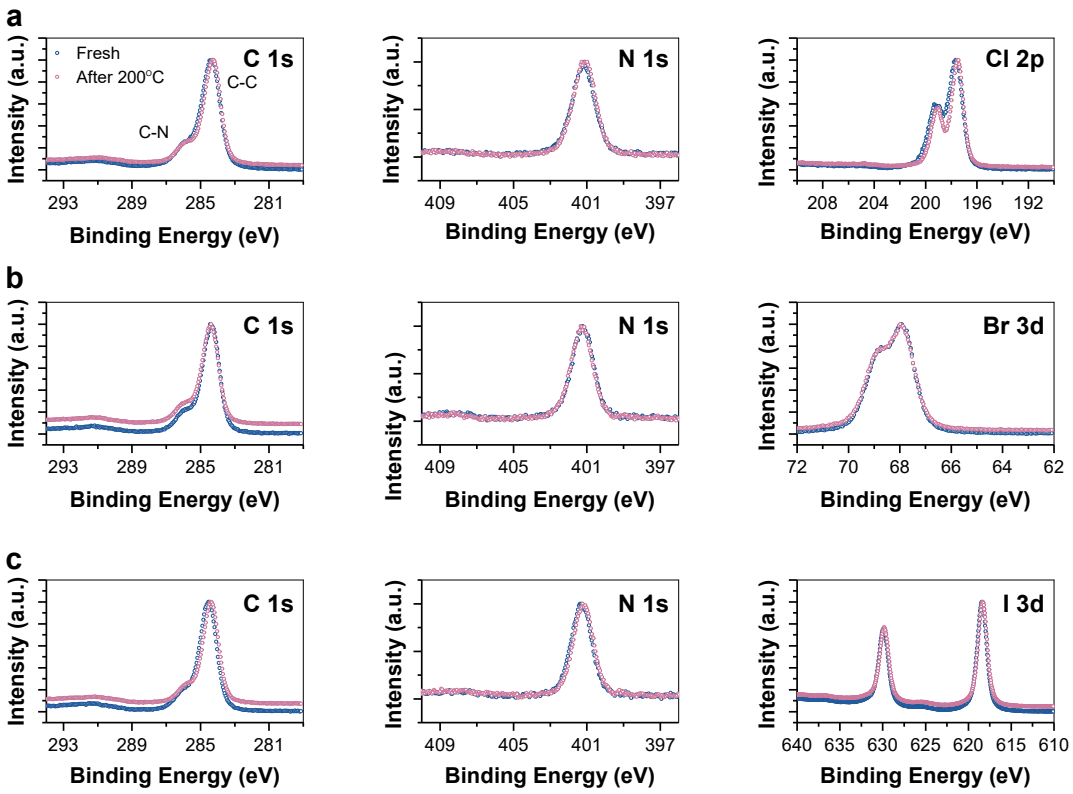

Fig. S9. C 1s, N 1s, and halogen core level XPS spectra of halogenated PEA organic powders before (fresh) and after heating from room temperature to 200ºC in an Ar atmosphere. **a**, PEACl. **b**, PEABr. **c**, PEAI.

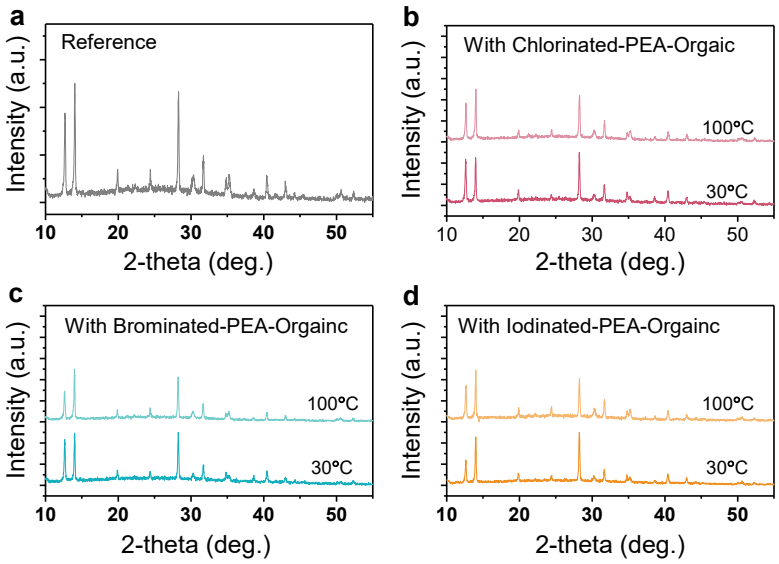

Fig. S10. The XRD patterns of the perovskite without (reference) and with the halogenated PEA organic. **a**, Reference. **b**, The perovskite was treated with the chlorinated PEA organic. **c**, The perovskite was treated with the brominated PEA organic. **d**, The perovskite was treated with iodinated PEA organics.

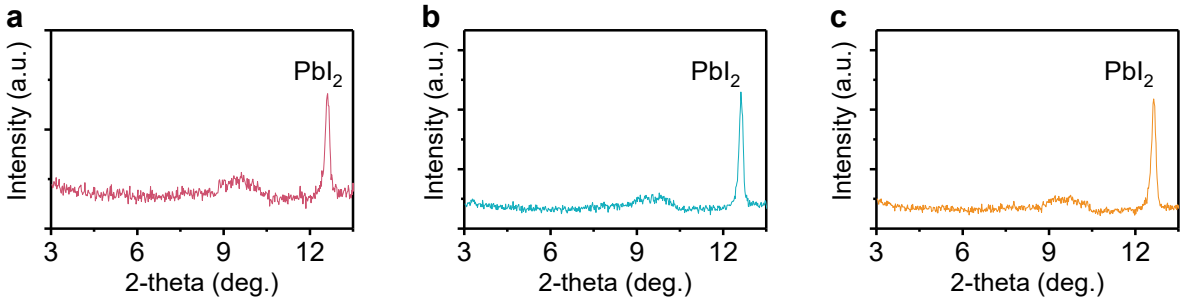

Fig. S11. The expanded view of XRD patterns at the low 2θ region. **a**, The perovskite with the chlorinated PEA organic. **b**, The perovskite with the brominated PEA organic. **c**, The perovskite with the iodinated PEA organic. XRD patterns did not show 2D or reduced dimensional perovskites patterns for all samples.

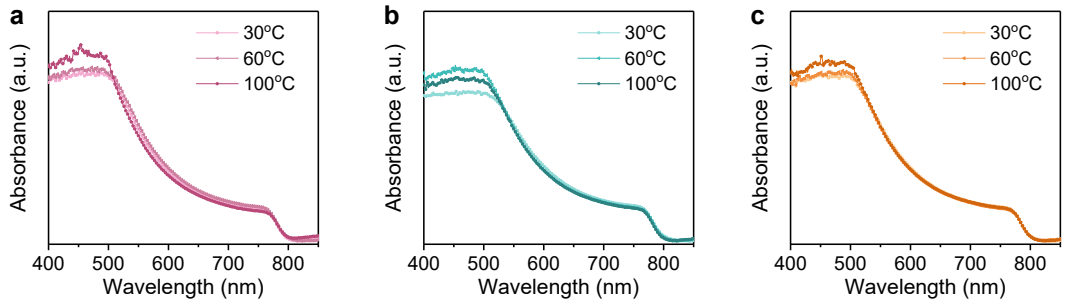

Fig. S12. UV-vis absorption spectra of the perovskite with different organics under varied temperatures. **a**, The perovskite with the chlorinated PEA organic. **b**, The perovskite with the brominated PEA organic. **c**, The perovskite with the iodinated PEA organic. The perovskite films, with the different temperature treatments that include varying the organic layers and changes to the temperature, exhibit identical band edge onsets. The variation in the 400-500 nm may result from changes to the optical reflection of perovskite surfaces with thermally-activated organics sublimation as samples are excited from the perovskite surface side.

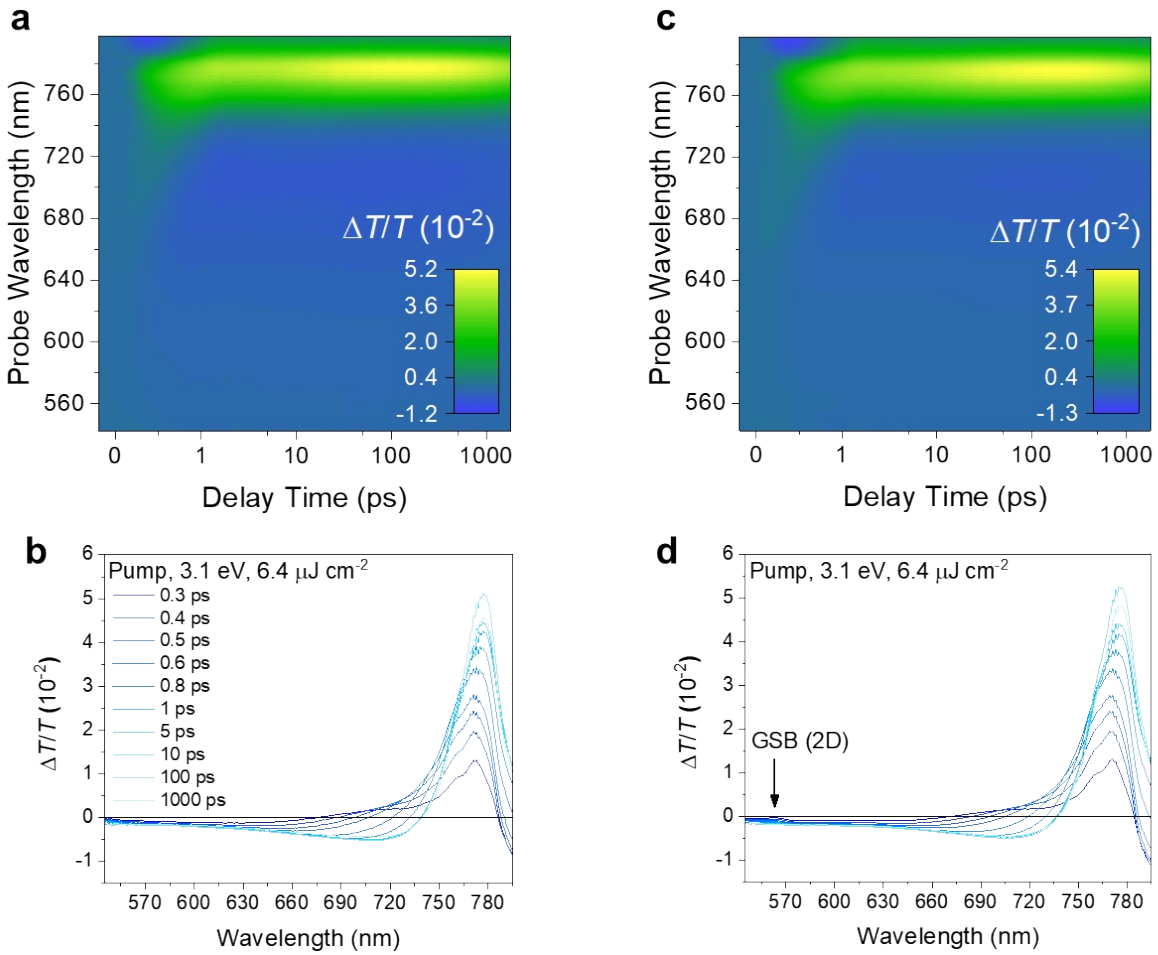

Fig. S13. Transient absorption (TA) spectroscopy of perovskite films without and with the halogenated PEA organic. TA maps and corresponding TA spectra of (**a** and **b**) the control perovskite and (**c** and **d**) the perovskite treated with the iodinated PEA organic, respectively. GSB, ground-state bleach. (Pump, 400 nm, 6.4 μJ cm^{-2})

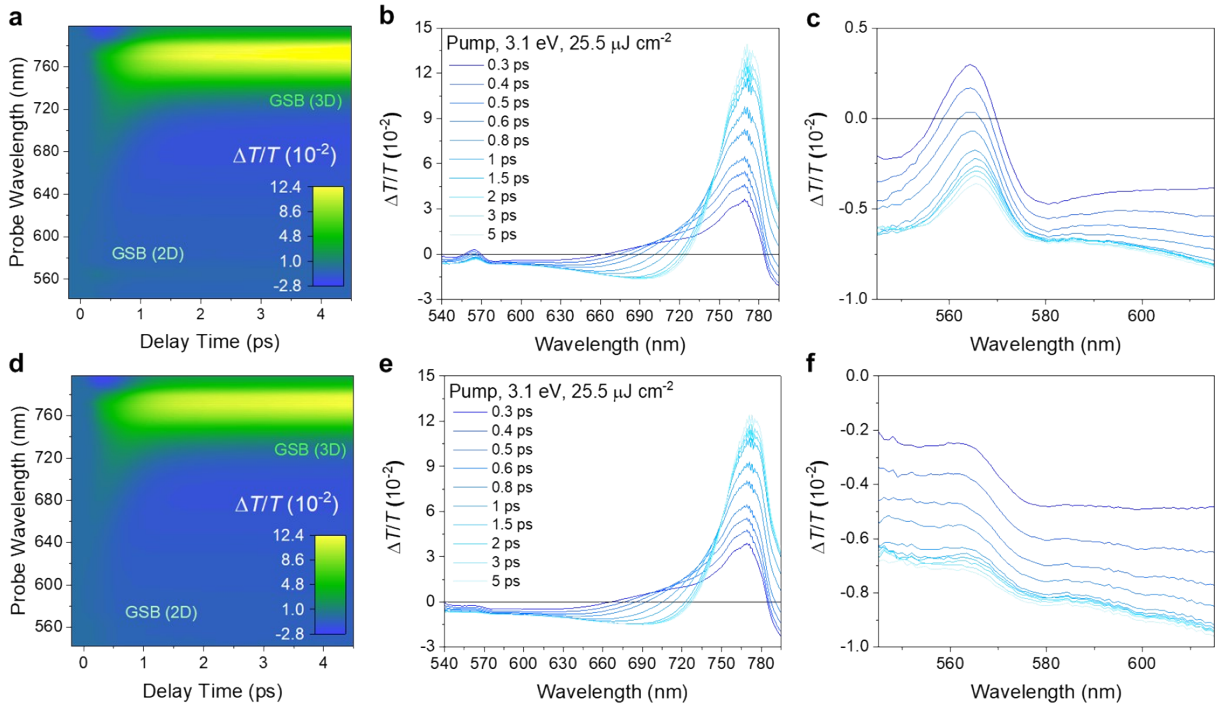

Fig. S14. Transient absorption (TA) spectroscopy of perovskite films. TA maps and corresponding TA spectra of (**a-c**) the perovskite treated with the chlorinated PEA organic, and (**d-f**) the perovskite treated with the iodinated PEA organic, respectively. GSB, ground-state bleach. (Pump, 400 nm, 25.5 μJ cm^{-2}).

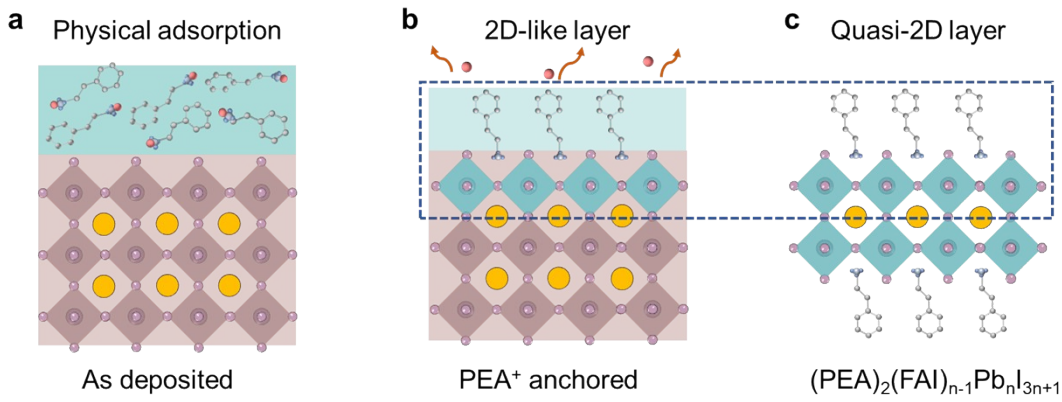

Fig. S15. Schematic diagram of perovskite grain surfaces with halogen-cleaved PEA^+ anchoring. **a**, As-deposited halogenated PEA organics on the perovskite. **b**, 2D-like perovskite formed on the surface. **c**, Schematic diagram of the quasi-2D perovskite.

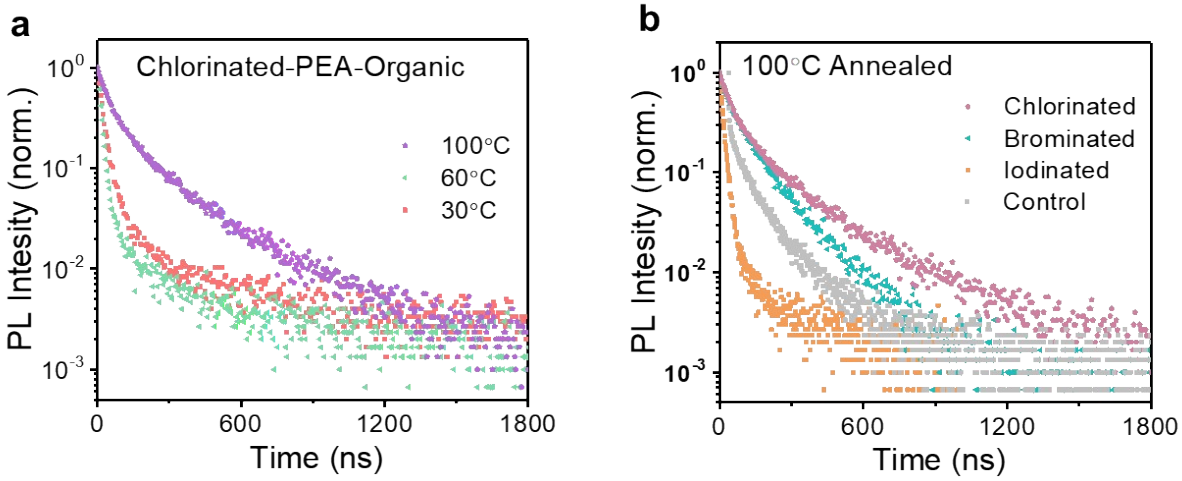

Fig. S16. Time-resolved photoluminescence (TRPL) decays. **a**, Comparing TRPL decays for the perovskites with the chlorinated PEA organic annealed at 30℃, 60℃, and 100℃. **b**, TRPL decays for the perovskite with and without (Control) the varied halogenated PEA organic annealed at 100℃.

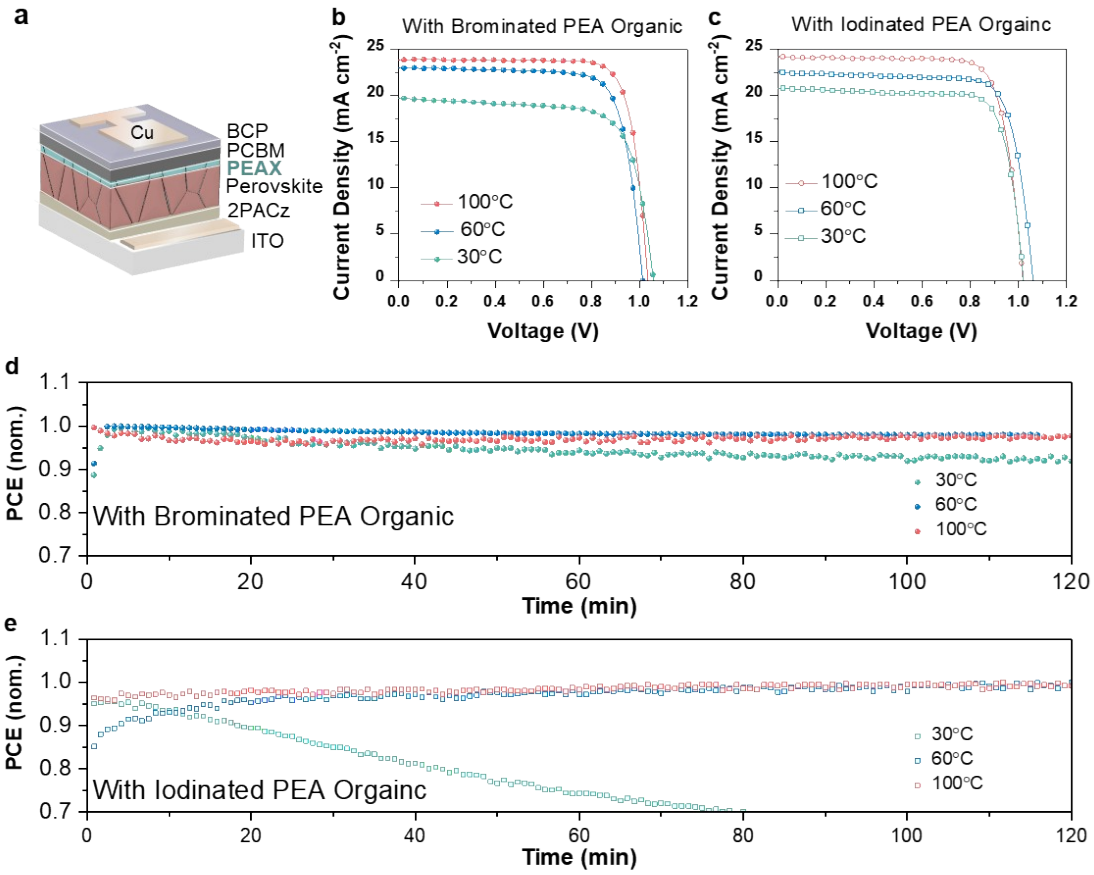

Fig. S17. Photovoltaic performances of PSCs with halogenated PEA organic ligands. **a**, Device configuration schematic of positive-intrinsic-negative PSCs. At different temperatures, *J-V* curves of PSCs with the brominated- **b**, and **c**, iodinated-PEA-organic ligands. Continuous MPP tracking under the full AM 1.5G illumination for the PSCs with brominated- **d**, and **e**, iodinated-PEA-organic ligands at different temperatures.

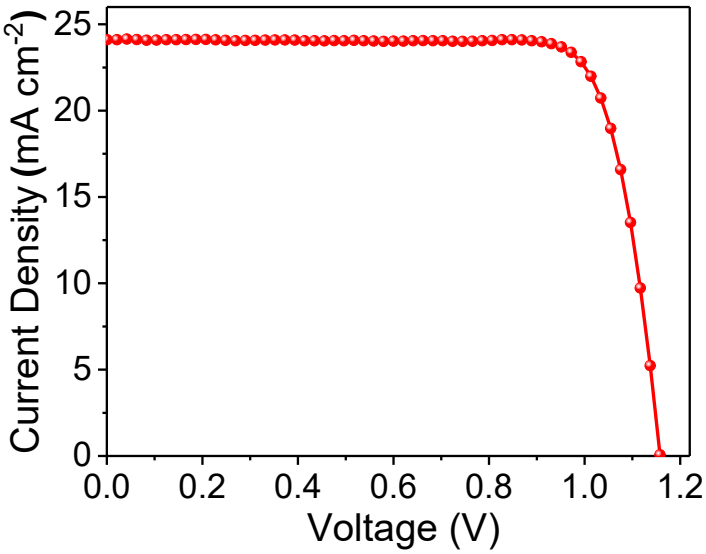

Fig. S18. Current density-voltage characteristics of the champion PSCs processed with Cl-cleaved PEA^+ anchoring. The device consists of ITO/NiO/2PACz/perovskite/PCBM/BCP/Cu. The device presents a power conversion efficiency of 23.1% (a short current density of 24.28 mA cm^{-2}, an open-circuit voltage of 1.16 V, and a fill factor of 82%).

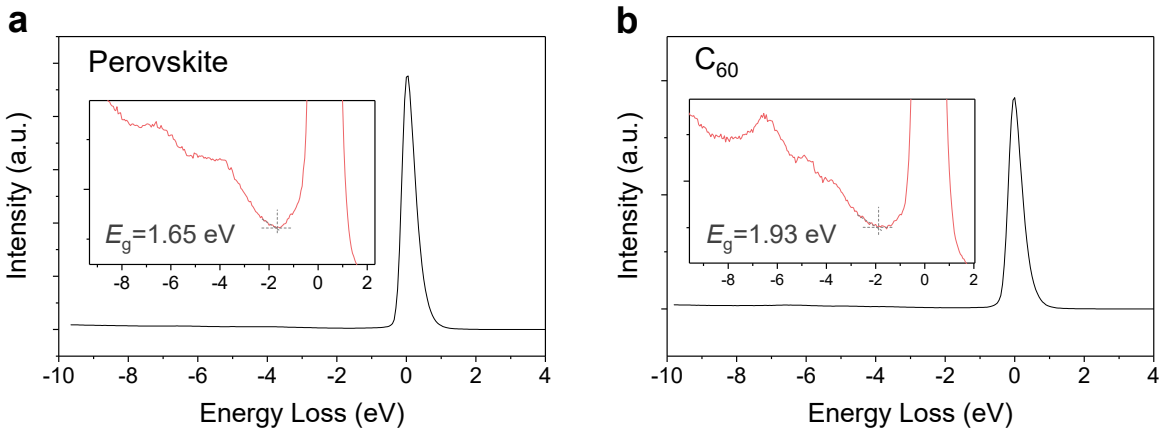

Fig. S19. REELS spectra of the perovskite and C_{60} film. The surface bandgap (E_g) of both **a**, the perovskite and **b**, C_{60} electron extraction layer is 1.65 eV and 1.93 eV, respectively.

Table S1. Photovoltaic performances of PSCs processed with halogenated PEA organics at different temperatures. The device fabricated with the chlorinated PEA organic treatment exhibits the highest power conversion efficiency among these PSCs below.

Treatment	Annealing Temp (°C)	V_{OC} (V)	J_{SC} (mA/cm^2)	FF	PCE (%)
W/O	N/A	1.008	23.11	0.77	17.95
Chlorinated PEA	30	1.073	15.34	0.56	9.23
	60	1.104	20.28	0.77	17.27
	100	**1.110**	**23.79**	**0.83**	**21.91**
Brominated PEA	30	1.060	19.78	0.73	15.35
	60	1.016	23.07	0.77	18.14
	100	1.039	23.72	0.82	20.20
Iodinated PEA	30	1.063	22.47	0.79	18.87
	60	1.026	20.94	0.79	16.94
	100	1.022	24.16	0.80	19.69

Table S2. The area ratios of C-C and C-N bond of halogenated PEA organics with various thermal treatments range from 30°C to 100°C. The ratios of C-C and C-N for three kinds of samples processed with various halogenated PEA organics are rarely changed when increasing the temperature, which excludes the possibility of chemical decomposition of halogenated PEA organics themselves at the elevated temperature.

	C-C: C-N		
	Chlorinated PEA	**Brominated PEA**	**Iodinated PEA**
30℃	86.7:13.3	85.9:14.1	86.1:13.9
40℃	87.0:13.0	86.4:13.6	86.9:13.1
50℃	85.9:14.2	86.2:13.7	86.1:13.9
60℃	86.8:13.2	86.8:13.2	87.0:13.0
70℃	86.8:13.2	86.4:13.6	86.1:13.9
80℃	85.2:14.8	86.6:13.4	87.1:12.9
100℃	87.2:12.8	86.8:13.3	86.8:13.2

Table S3. The atomic ratios of N and halogen of the halogenated PEA organic powder before and after 200°C heating in an Ar atmosphere. These data show no notable decomposition happening upon thermal treatment at 200°C.

		Atomic Ratio N: Halogen
PEACl	Fresh	51.1:48.9
	After 200°C	51.2:48.8
PEABr	Fresh	51.0:49.0
	After 200°C	50.7:49.3
PEAI	Fresh	49.4:50.6
	After 200°C	48.9:51.1

Table S4. Summary of best-performing PSCs with surface organic treatments reported in the literature. Most of the device efficiencies reported are certified by independent certification labs.

Devices	Perovskite	Eff. (%)	Treatments	Ref.
p-i-n	$FA_{1-x-y}MA_xCs_yPbI_{3-z}Br_z$	23.7 (certified)	Liquid medium(anisole) annealing (LMA)	4
p-i-n	$Cs_{0.05}(FA_{5/6}MA_{1/6})_{0.95}Pb(I_{0.85}Br_{0.15})_3$	23.7	4-fluorophenylethylammonium iodide (F-PEAI)	5
p-i-n	$\mathbf{Cs_{0.15}FA_{0.85}Pb(I_{0.95}Br_{0.05})_3}$	22.3 (certified)	Poly(triarylamine) (p-PY) as HTL, PEAI modified pervoskite surface	6
p-i-n	$(CsPbI_3)_{0.05}[FA_{0.85}MA_{0.15}Pb(I_{0.85}Br_{0.15})_3]_{0.95}$	22.31	1,4-butanediammonium iodide (BDAI)	7
p-i-n	$Cs_{0.05}(FA_{0.95}MA_{0.05})_{0.95}Pb(I_{0.95}Br_{0.05})_3$	22.7 (certified)	Piperazinium iodide (PI)	8
p-i-n	$(FAPbI_3)_{0.95}(MAPbBr_3)_{0.05}$	>24	Lead-sulfur	9
p-i-n	$(FA_{0.98}MA_{0.02})_{0.95}Cs_{0.05}Pb(I_{0.95}Br_{0.02})_3$	25.0	Ferrocenyl-bis-thiophene-2-carboxylate ($FcTc_2$)	10
n-i-p	$(FAPbI_3)_x(MAPbBr_3)_{1-x}$	23.0	Ethylammonium (PREA)	11
n-i-p	$FAPbI_3$	25.5 (certified)	Cl-bonded SnO_2& a Cl-containing perovskite precursor [methylenediamine dihydrochloride ($MDACl_2$)]	12
n-i-p	$FAPbI_3$	25.2 (certified)	Formamidine formate (FAHCOO)	13
n-i-p	$\mathbf{FA_{0.9}Cs_{0.1}PbI_3}$	23.25	Imidazole hydrobromide (IABr)	14
n-i-p	$FAPbI_3$	24.1	Ionic liquid methylamine formate (MAFa)	15
n-i-p	$FAPbI_3$	25.2 (certified)	$MAPbBr_3$ additive	16

n-i-p	$(FAPbI_3)_x(MACl)_y$	25.4 (certified)	Polyacrylic acid-stabilized tin (IV) oxide quantum dots (paa-QD-SnO_2@c-TiO_2)	[17]
n-i-p	$FAPbI_3$	24.64	Fluorinated isomeric analogs (Spiro-mF) of Spiro-OMeTAD	[18]
n-i-p	$(FAI)_{10}$ $(MABr)_1$ $(MACl)_1$	23.5	A-site doping of Cs^+ and GA^+ cations (guanidinium) in $FAPbI_3$	[19]
n-i-p	$FAPbI_3$	23.9	Isopropylammonium chloride (iPAmHCl) added to the $FAPbI_3$ precursor solution	[20]
n-i-p	$Cs_{0.05}(FA_{0.85}MA_{0.15})_{0.95}Pb(I_{0.85}Br_{0.15})_3$	21.4	3-iodopropyl trimethoxysilane $[Si(OCH_3)_3(CH_2)_3I]$ I-SAM	[21]
n-i-p	$(FAPbI_3)_{0.95}(MAPbBr_3)_{0.05}$	22.7 (certified)	n-hexyl trimethyl ammonium bromid	[22]
n-i-p	$FAPbI_3$	23.7 (certified)	Methylenediammoniumdichloride ($MDACl_2$) dope in $FAPbI_3$	[23]

References

1. in *An Introduction to Surface Analysis by XPS and AES*, 2003, DOI: https://doi.org/10.1002/0470867930.ch4, pp. 79-111.
2. M. P. Seah, *Surf. Interface Anal.*, 2012, **44**, 1353-1359.
3. Z. H. Lu, J. P. McCaffrey, B. Brar, G. D. Wilk, R. M. Wallace, L. C. Feldman and S. P. Tay, *Appl. Phys. Lett.*, 1997, **71**, 2764-2766.
4. N. Li, X. Niu, L. Li, H. Wang, Z. Huang, Y. Zhang, Y. Chen, X. Zhang, C. Zhu, H. Zai, Y. Bai, S. Ma, H. Liu, X. Liu, Z. Guo, G. Liu, R. Fan, H. Chen, J. Wang, Y. Lun, X. Wang, J. Hong, H. Xie, D. S. Jakob, X. G. Xu, Q. Chen and H. Zhou, *Science*, 2021, **373**, 561-567.
5. M. Degani, Q. An, M. Albaladejo-Siguan, Y. J. Hofstetter, C. Cho, F. Paulus, G. Grancini and Y. Vaynzof, *Sci. Adv.*, 2021, **7**, eabj7930.
6. R. Chen, S. Liu, X. Xu, F. Ren, J. Zhou, X. Tian, Z. Yang, X. Guanz, Z. Liu, S. Zhang, Y. Zhang, Y. Wu, L. Han, Y. Qi and W. Chen, *Energy Environ. Sci.*, 2022, **15**, 2567-2580.
7. S. Wu, J. Zhang, Z. Li, D. Liu, M. Qin, S. H. Cheung, X. Lu, D. Lei, S. K. So, Z. Zhu and A. K. Y. Jen, *Joule*, 2020, **4**, 1248-1262.
8. F. Li, X. Deng, F. Qi, Z. Li, D. Liu, D. Shen, M. Qin, S. Wu, F. Lin, S. H. Jang, J. Zhang, X. Lu, D. Lei, C. S. Lee, Z. Zhu and A. K. Jen, *J. Am. Chem. Soc.*, 2020, **142**, 20134-20142.
9. X. Li, W. Zhang, X. Guo, C. Lu, J. Wei and J. Fang, *Science*, 2022, **375**, 434-437.
10. Z. Li, B. Li, X. Wu, S. A. Sheppard, S. Zhang, D. Gao, N. J. Long and Z. Zhu, *Science*, 2022, **376**, 416-420.
11. J. Xue, R. Wang, X. Chen, C. Yao, X. Jin, K. L. Wang, W. Huang, T. Huang, Y. Zhao, Y. Zhai, D. Meng, S. Tan, R. Liu, Z. K. Wang, C. Zhu, K. Zhu, M. C. Beard, Y. Yan and Y. Yang, *Science*, 2021, **371**, 636-640.
12. H. Min, D. Y. Lee, J. Kim, G. Kim, K. S. Lee, J. Kim, M. J. Paik, Y. K. Kim, K. S. Kim, M. G. Kim, T. J. Shin and S. Il Seok, *Nature*, 2021, **598**, 444-450.
13. J. Jeong, M. Kim, J. Seo, H. Lu, P. Ahlawat, A. Mishra, Y. Yang, M. A. Hope, F. T. Eickemeyer, M. Kim, Y. J. Yoon, I. W. Choi, B. P. Darwich, S. J. Choi, Y. Jo, J. H. Lee, B. Walker, S. M. Zakeeruddin, L. Emsley, U. Rothlisberger, A. Hagfeldt, D. S. Kim, M. Gratzel and J. Y. Kim, *Nature*, 2021, **592**, 381-385.
14. C. Wang, X. Wang, Z. He, B. Zhou, D. Qu, Y. Wang, H. Hu, Q. Hu and Y. Tu, *Chem. Eng. J.*, 2022, **444**.
15. W. Hui, L. Chao, H. Lu, F. Xia, Q. Wei, Z. Su, T. Niu, L. Tao, B. Du, D. Li, Y. Wang, H. Dong, S. Zuo, B. Li, W. Shi, X. Ran, P. Li, H. Zhang, Z. Wu, C. Ran, L. Song, G. Xing, X. Gao, J. Zhang, Y. Xia, Y. Chen and W. Huang, *Science*, 2021, **371**, 1359-1364.
16. J. J. Yoo, G. Seo, M. R. Chua, T. G. Park, Y. Lu, F. Rotermund, Y. K. Kim, C. S. Moon, N. J. Jeon, J. P. Correa-Baena, V. Bulovic, S. S. Shin, M. G. Bawendi and J. Seo, *Nature*, 2021, **590**, 587-593.
17. M. Kim, J. Jeong, H. Lu, T. K. Lee, F. T. Eickemeyer, Y. Liu, I. W. Choi, S. J. Choi, Y. Jo, H. B. Kim, S. I. Mo, Y. K. Kim, H. Lee, N. G. An, S. Cho, W. R. Tress, S. M. Zakeeruddin, A. Hagfeldt, J. Y. Kim, M. Gratzel and D. S. Kim, *Science*, 2022, **375**, 302-306.
18. M. Jeong, I. W. Choi, E. M. Go, Y. Cho, M. Kim, B. Lee, S. Jeong, Y. Jo, H. W. Choi, J. Lee, J. H. Bae, S. K. Kwak, D. S. Kim and C. Yang, *Science*, 2020, **369**, 1615-1620.
19. M. Qin, H. Xue, H. Zhang, H. Hu, K. Liu, Y. Li, Z. Qin, J. Ma, H. Zhu, K. Yan, G. Fang, G. Li, U. S. Jeng, G. Brocks, S. Tao and X. Lu, *Adv. Mater.*, 2020, **32**, e2004630.
20. B.-w. Park, H. W. Kwon, Y. Lee, D. Y. Lee, M. G. Kim, G. Kim, K.-j. Kim, Y. K. Kim, J. Im, T. J. Shin and S. I. Seok, *Nat. Energy*, 2021, **6**, 419-428.
21. Z. Dai, S. K. Yadavalli, M. Chen, A. Abbaspourtamijani, Y. Qi and N. P. Padture, *Science*, 2021, **372**, 618-622.
22. E. H. Jung, N. J. Jeon, E. Y. Park, C. S. Moon, T. J. Shin, T. Y. Yang, J. H. Noh and J. Seo, *Nature*, 2019, **567**, 511-515.
23. H. Min, M. Kim, S. U. Lee, H. Kim, G. Kim, K. Choi, J. H. Lee and S. I. Seok, *Science*, 2019, **366**, 749-753.